Serrano, J.; Arnau Martínez, FJ.; García-Cuevas González, LM.; Inhestern, LB. (01-0). An innovative losses model for efficiency map fitting of vaneless and variable vaned radial turbines extrapolating towards extreme off-design conditions. Energy. 180:626-639. https://doi.org/10.1016/j.energy.2019.05.062

J. R. Serrano, F. J. Arnau, L. M. García-Cuevas, L. B. Inhestern, An innovative losses model for efficiency map fitting of vaneless and variable vaned radial turbines extrapolating towards extreme off-design conditions, Energy 180 (2019) 626–639. doi:10.1016/j.energy.2019.05.062

An Innovative Losses Model for Efficiency Map Fitting of Vaneless and Variable Vaned Radial Turbines Extrapolating Towards Extreme Off-Design Conditions

José Ramón Serrano[a], Francisco Jose Arnau Martínez[a,*], Luis Miguel García-Cuevas[a], Lukas Benjamin Inhestern[a]

[a] *CMT-Motores Térmicos, Universitat Politècnica de València, Valencia 46022, Spain.*

Abstract

Pulsating flow in automotive turbocharger turbines makes it necessary to know performance characteristics in difficult to measure off-design conditions. Physically based extrapolation models can be used to extrapolate towards unmeasured map regions. However, for model parameter fittings common maps have low numbers of measurement points per speedline available. Measurements with different variable geometry turbine (VGT) openings amplify the available data and help to characterize the turbine in a wider aerodynamic range. Nevertheless, physical models able to fit the data of several speeds and VGT positions with the same set of fitting parameters are rare. Thus, a model that is capable of fitting all speeds and VGT positions simultaneously and with the capability of extrapolating reliably towards low pressure ratios, unmeasured speeds, and VGT openings has been developed. The model is based on novel and commonly used loss correlations combined in an innovative way and has been validated in a wide range of pressure ratios towards extreme off-design conditions. By deactivating stator passage effects, the model can also extrapolate efficiency maps of vaneless turbines. The set of loss models is able to reproduce the measured data in a good quality for tested turbines with a very reduced number of fitting coefficients.

Keywords: Turbocharger, Model, Extrapolation model, Radial turbine simulation, Off-design, High BSR

*Corresponding author. Tel: +34963877650; fax: +34963877659
Email address: farnau@mot.upv.es (Francisco Jose Arnau Martínez)
URL: www.cmt.upv.es (Francisco Jose Arnau Martínez)

1. Introduction

Current trends in petrol engines development are affected by downsizing. By rising the engine inlet pressure, less volume is needed for reaching optimum brake mean effective pressure (BMEP). Thus, spark ignition engines can be designed lighter and have less friction losses. To fulfill the needs of compressed inlet air, turbochargers are commonly used. In the design process of engines they are often simulated by means of one-dimensional models, where the turbocharger turbine and compressor are modeled by one-dimensional or zero-dimensional sub-models [1]. These models, like the ones by Rajoo et al. [2], Chiong et al. [3], or Galindo et al. [4], are usually fitted with the data of turbine and compressor maps measured in stationary conditions. However, turbine maps consist of running points in a rather narrow range, measured under stationary conditions [5].

Due to periodically tightened emission regulations (E6, E6d+RDE, US-FTP, ...) [6] highly dynamic and real driving cycles are put into the focus of engine developer. Under the conditions of dynamic urban driving the engine operates at rather low loads and frequently decelerating and accelerating engine speed. Consequently, the mean air mass flow changes quickly and the turbocharger operates under pulsating mass flow conditions far away from the design point and from the typically measured points [7]. Off-design refers to the conditions very far from peak efficiency that were very probably not taken into consideration in the turbine design. But they are indeed important because the turbine works at these conditions during significant part of the pressure pulse period in pulsating flow operation [8]. Thus, this off-design operating conditions are of high interest for engine designers to predict engine-turbocharger matching. However, due to the turbine braking power restriction of compressors choke and surge limitation, this conditions cannot be measured in traditionally used turbocharger test benches. In the literature, approaches like the one by Salameh et al. [9] or Serrano et al. [10, 11] are recommended to measure in a wide range of turbine running points towards low blade to jet speed ratios (BSRs) but are not commonly used in the industry yet. Furthermore, apart of limiting rotational speeds, the inherent measurement error is rather high at certain running conditions with low turbine mass flow and low rotational speed [10]. Furthermore, these measurement methods are often restricted by a maximum rotational speed

making the extrapolation capability towards higher rotational speeds a valuable quality of an extrapolation model. Due to high inherent measurement uncertainties when measuring small power outputs at low pressure ratios, efficiency extrapolations towards low rotational speeds are also of high interest to verify measured data.

When only narrow maps are available, extrapolation models have to be used to obtain data in unmeasured regions (high BSR/ high speeds) of the map. In the recent past much effort has been put into extrapolating the turbocharger maps mainly in terms of high BSRs (low mass flows) [12, 13, 14, 15, 16]. However, extrapolations towards lower and higher rotational speeds combined with extrapolating towards high BSR have not been in the focus yet. Also, extrapolations towards unmeasured VGT positions like performed by Serrano et al. [15], can rarely been found in the literature. To allow this kind of extrapolation, models able to fit the data of different VGT positions with one set of coefficients are required. Additionally, such a fitting ability allows to use more available data as input information for the model. Following, it is expected to achieve more reliable model fittings over a wide range of pressure ratios. Using physical efficiency models is expected to improve the extrapolation quality and reliability in comparison to semi-empirical ones like the one by Serrano et al. [15] or by Martins et al. [17]. Fitting the physical behavior of the turbine over different VGT positions demands new loss modeling in the stator passage and the vaneless space.

One risk in physical one-dimensional turbine modeling and the fitting of model parameters is the overestimation of rather small and unimportant aerodynamic effects. Thus, adding increasing numbers of submodels with including fitting parameters simplifies the curve fit of the given data but also might misjudge the extrapolated zones of the map. Hence, an equilibrium of the degree of detail and simplicity is of high importance. Furthermore, a growing number of fitting coefficients requires an increasing number of data points. Hence, it should be tried to reach low numbers of empirically fitted parameters.

Due to the small geometry of turbochargers from downsized engines, heat transfer affects significantly the efficiency of the turbine and compressor, especially in operating conditions at low loads [18]. Therefore, the required models have to take heat flux into account or the maps have to be adiabatized before extrapolation like shown in [19]. By using the procedure of Sirakov and Casey [20], Serrano et al. [21], Zimmermann et al. [22], or Serrano et al. [11] maps can be adiabatized, so that a simple adiabatic turbine model can

be used for map extrapolation.

This paper presents an adiabatic turbine efficiency model, which has the ability to extrapolate towards lower and higher speeds at the same time with extrapolating towards extremely high BSRs. Furthermore, the model is designed to fit different VGT positions at the same time and to extrapolate towards unmeasured positions. The here presented physically based model is designed with commonly used and with novel loss correlations in rotor and stator. The tip leakage model presented in [23] is applied for the first time in a complete turbine efficiency model.

First, the model and its working principle is presented. Following, the model fitting is validated by means of various radial turbine maps. Further, the extrapolation in BSR, in shaft speed, and in VGT positioning is compared with maps of one turbocharger measured in a wide range of BSRs. Finally, results are discussed and concluded.

2. Turbine Model

In the following, the design of a novel mean line model for steady, nonreactive flow is described. In the extrapolated regions of the map towards high BSRs the Mach number is rather low. Although the flow in this condition can be seen as incompressible, extrapolation models are usually fitted with running points measured at high mass flows and Mach numbers. Thus, the gas compressibility has to be taken into account in most parts of the model. The developed extrapolation model has been designed for turbocharger radial turbines with variable guide vanes. The used nomenclature for turbines equipped with stator blades can be seen in Figure 1. The model can also be used for vaneless turbines when the stator passage is taken out of the model. Thus, for vaneless turbines stations $2'$ and 2 are not considered and the outlet values of the volute define the inlet condition of the vaneless space.

Dividing nominator and denominator of the total-to-static efficiency equation with the total inlet enthalpy $h_{\mathrm{t},0}$ the following equation has been obtained:

$$\eta_{\mathrm{ts}} = \frac{\frac{h_{\mathrm{t},3}}{h_{\mathrm{t},0}} - \frac{h_{\mathrm{t},4}}{h_{\mathrm{t},0}}}{\frac{h_{\mathrm{t},0}}{h_{\mathrm{t},0}} - \frac{h_{5,\mathrm{s}}}{h_{\mathrm{t},0}}}. \tag{1}$$

Here, non-dimensional numbers appear when the kinetic energy or the enthalpy losses are divided by the total inlet enthalpy. The relative enthalpy change along the turbine can be represented as in Figure 2 for stator and

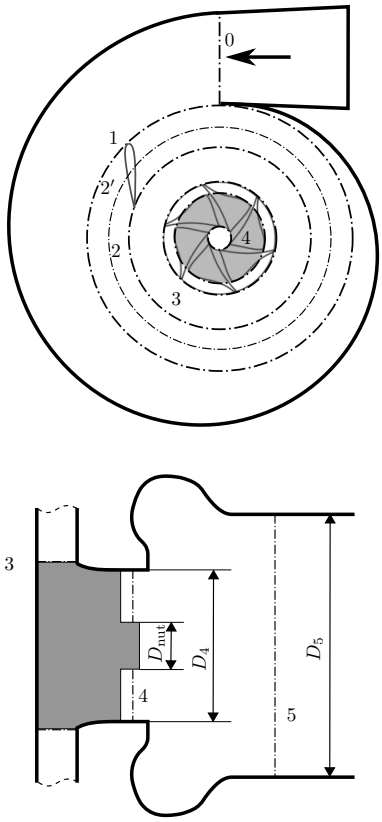

Figure 1: Turbine section nomenclature.

vaneless space and in Figure 3 for rotor and outlet. All losses have been modeled as relative enthalpy losses. The entire model has been developed

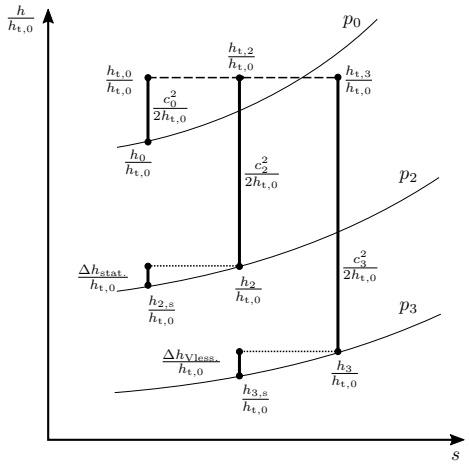

Figure 2: Stator and vaneless space enthalpy.

with these non-dimensional numbers. This way no inlet temperature has to be assumed for the calculation of the efficiency based on reduced map numbers. Furthermore, the calculation of the density, which might require extra iterations in compressible models, can be omitted at all parts of the model. Additionally, the number of necessary iterations within the model can be reduced even more, since used loss models depend linearly on relative kinetic energies.

In common turbocharger test benches the total temperature is calculated with the static temperature and meridional velocity coming from mass flow measurements. Since the swirl is very high in the outlet duct when measuring in extreme off-design conditions, the kinetic energy of the tangential velocity component needs to be added. This way the experimentally measured efficiency can be modeled. (In a further step the efficiency considering the full kinetic energy in the turbine outlet can be calculated.) Thus, the efficiency can be deduced from Figure 3 as:

$$\eta_{\mathrm{ts}} = \frac{1 - \left(\frac{p_4}{p_{\mathrm{t},3}}\right)^{\frac{\gamma-1}{\gamma}} - \frac{c_{5,\mathrm{m}}^2}{2 \cdot h_{\mathrm{t},0}} - \frac{\Delta h_{\mathrm{loss,rot}}}{h_{\mathrm{t},0}} - \frac{\Delta h_{\mathrm{loss,rot,tip}}}{h_{\mathrm{t},0}}}{1 - \left(\frac{p_5}{p_{\mathrm{t},0}}\right)^{\frac{\gamma-1}{\gamma}}}. \tag{2}$$

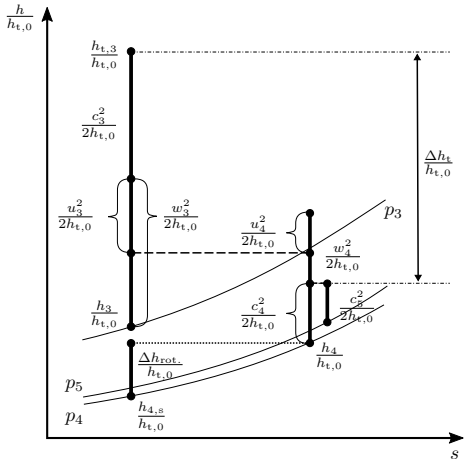

Figure 3: Rotor enthalpy.

Here, the pressure ratio $\frac{p_{t,0}}{p_5}$ is the overall pressure ratio ($\pi_{\text{turb.}}$) that can be measured; $\frac{p_{t,3}}{p_4}$ is the rotor pressure ratio. The unknown rotor pressure ratio has been calculated from the stator pressure ratio, the pressure ratio over the vaneless space, the outlet pressure ratio and the overall pressure ratio:

$$\frac{p_{t,3}}{p_4} = \frac{\frac{p_{t,0}}{p_5}}{\frac{p_{t,0}}{p_{t,2}} \cdot \frac{p_{t,2}}{p_{t,3}} \cdot \frac{p_4}{p_5}}. \tag{3}$$

To calculate the unknown numbers in Equation 2 and Equation 3, the turbine zones have been solved partwise. The turbine has been split into volute (0-1), stator passage (1-2), vaneless space (2-3), rotor passage (3-4), and outlet region with diffuser (4-5). The modeling of each turbine section is shown in the following.

2.1. Volute

Due to the relatively low velocities, the losses in the volute have been assumed as rather low in comparison to the losses in stator, vaneless space, and rotor. Thus, the losses have been neglected and the flow angle has been calculated from mass flow and momentum conservation:

$$\alpha_1 = atan\left(\frac{8 \cdot r_0 \cdot H_1}{D_0^2}\right). \tag{4}$$

Where D_0 is the diameter of the volute inlet (0); r_0 the radius from the rotor center to the middle point of the Volute inlet; H_1 the nozzle inlet height. The

meridional velocity in the stator inlet (1) can be calculated from the reduced mass flow:

$$\frac{c_{1,\mathrm{m}}^2}{2 \cdot h_{\mathrm{t},0}} = \frac{R^2 \cdot \dot{m}_{\mathrm{red.}}^2}{A_1^2 \cdot c_{\mathrm{p}} \cdot 2}, \tag{5}$$

$$\frac{c_1^2}{2 \cdot h_{\mathrm{t},0}} = \frac{c_{1,\mathrm{m}}^2}{2 \cdot h_{\mathrm{t},0} \cdot cos\left(\alpha_1\right)} \tag{6}$$

Thus, the stator inlet condition is fully defined.

2.2. Stator

To obtain a consistent set of fitting coefficients for all VGT positions at the same time, the moving mechanism of the stator vanes has to be modeled properly. First a linear correlation between vane opening percentage and stator blade angle has been assumed as it has been stated by Serrano et al. [15]. To calculate the stator throat length $l_{\mathrm{thr.}}$ (blue dashed line in Figure 4) from the blade angle, the geometry can be resolved by means of the variables shown in Figure 4.

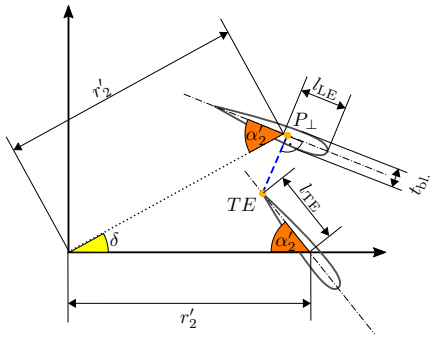

Figure 4: Stator throat (blue dashed line) calculation.

Using the known geometrical data a correlation between the stator vane angle and the throat area can be derived. This is done by calculating the position of the trailing edge of one vane (TE) and the closest point on the middle line of the next vane ($P_\perp$) in the indicated coordinate frame in Figure 4:

$$TE_x = r'_2 - l_{\mathrm{TE}} \cdot \cos(\alpha'_2), \tag{7}$$

$$TE_y = \sin(\alpha'_2) \cdot l_{\mathrm{TE}}, \tag{8}$$

$$P_{\perp,\mathrm{x}} = \frac{l_{\mathrm{TE}} \cdot \left(\sin(\delta) + \cos(\delta) \cdot \frac{-1}{\tan\left(\delta - \alpha_2'\right)} \right)}{\frac{1+\tan^2\left(\delta-\alpha_2'\right)}{\tan\left(\delta-\alpha_2'\right)}} - \\ - \frac{r_2' \cdot \left(\sin(\delta) - \tan(-\alpha_2' - \delta) \cdot \cos(\delta) + \frac{-1}{\tan\left(\delta-\alpha_2'\right)} \right)}{\frac{1+\tan^2\left(\delta-\alpha_2'\right)}{\tan\left(\delta-\alpha_2'\right)}}, \tag{9}$$

$$\text{with} : \delta = \frac{2 \cdot \pi}{z},$$

$$P_{\perp,\mathrm{y}} = \tan\left(\delta - \alpha_2'\right) \cdot r_2' \cdot \left(P_{\perp,\mathrm{x}} \cdot \sin(\delta) - \cos(\delta)\right), \tag{10}$$

$$l_{\mathrm{thr.}} = \sqrt{\left(TE_x - P_{\perp,\mathrm{x}}\right)^2 + \left(TE_y - P_{\perp,\mathrm{y}}\right)^2} - \frac{t_{\mathrm{bl.}}}{2}. \tag{11}$$

Furthermore, changing stator inlet radius and outlet radius can be estimated as:

$$r_1 = \sqrt{\left(r_2' + l_{\mathrm{LE}} \cdot \cos(\alpha_2')\right)^2 + \sin(\alpha_2')^2 \cdot l_{\mathrm{LE}}^2}, \tag{12}$$

$$r_2 = \sqrt{\left(r_2' - l_{\mathrm{TE}} \cdot \cos(\alpha_2')\right)^2 + \sin(\alpha_2')^2 \cdot l_{\mathrm{TE}}^2}. \tag{13}$$

Loss models have been used to model the flow evolution in the stator. The same types of losses as they were recommended for the rotor passage by Futral et al. [24] have been assumed for the stationary stator passage. Consequently, the stator takes incidence and passage losses into account:

$$\frac{\Delta h_{\mathrm{stat.}}}{h_{\mathrm{t},0}} = \frac{\Delta h_{\mathrm{stat.,inc.}}}{h_{\mathrm{t},0}} + \frac{\Delta h_{\mathrm{stat.,pas.}}}{h_{\mathrm{t},0}}. \tag{14}$$

In the non-dimensional formulation they can be formulated as:

$$\frac{\Delta h_{\mathrm{stat.,inc.}}}{h_{\mathrm{t},0}} = z_{\mathrm{stat.,inc.}} \cdot \sin^2 i_1 \cdot \frac{c_1^2}{2 \cdot h_{\mathrm{t},0}}, \tag{15}$$

$$\frac{\Delta h_{\mathrm{stat.,pas.}}}{h_{\mathrm{t},0}} = z_{\mathrm{stat.,pas.}} \cdot \left(\cos^2 i_1 \cdot \frac{c_1^2}{2 \cdot h_{\mathrm{t},0}} + \frac{c_2^2}{2 \cdot h_{\mathrm{t},0}} \right). \tag{16}$$

Here i_1 is the difference between the current inlet flow angle and the current stator vane angle. The incidence loss is modeled by the dissipation of the

kinetic energy orthogonal to the optimum flow angle, which is assumed to be at $i = 0$ in the stator. The passage loss model describes a loss proportional to the mean value of the remaining inlet kinetic energy and the passage outlet kinetic energy [24]. Following, the stator outlet velocity can be iteratively calculated with:

$$\dot{m}_{\text{red.}} = \sqrt{\frac{c_2^2}{2 \cdot h_{\text{t},0}} \cdot 2 \cdot c_{\text{p}}} \cdot \frac{\cos \alpha_{2'} \cdot A_2 \cdot C_{\text{d},2}}{R} \cdot \frac{p_{\text{t},2}}{p_{\text{t},0}}. \tag{17}$$

A discharge coefficient $C_{\text{d},2}$ has been introduced to take into account that the real flow in a stator is not homogeneously distributed. Thus, the whole flow is assumed to flow though an effective area.

Finally, the stator total pressure ratio has been calculated by dividing the isentropic pressure ratio $\frac{p_{\text{t},0}}{p_2}$ with the effective pressure ratio $\frac{p_{\text{t},2}}{p_2}$:

$$\frac{p_{\text{t},0}}{p_2} = \left(\frac{1}{1 - \frac{c_2^2}{2 \cdot h_{\text{t},0}} - \frac{\Delta h_{\text{stat.}}}{h_{\text{t},0}}} \right)^{\frac{\gamma}{\gamma - 1}}, \tag{18}$$

$$\frac{p_{\text{t},2}}{p_2} = \left(\frac{1}{1 - \frac{c_2^2}{2 \cdot h_{\text{t},0}}} \right)^{\frac{\gamma}{\gamma - 1}}, \tag{19}$$

$$\frac{p_{\text{t},0}}{p_{\text{t},2}} = \left(\frac{1 - \frac{c_2^2}{2 \cdot h_{\text{t},0}}}{1 - \frac{c_2^2}{2 \cdot h_{\text{t},0}} - \frac{\Delta h_{\text{stat.}}}{h_{\text{t},0}}} \right)^{\frac{\gamma}{\gamma - 1}}. \tag{20}$$

2.3. Vaneless Space

It has been found out that the modeling of the vaneless space and its losses have a sensitive impact on the fitting of all VGT maps at the same time. Thus, the vaneless space had to be modeled as an additional nozzle. The corresponding loss has been formulated depending on flow length and velocity as:

$$\frac{\Delta h_{\text{Vless}}}{h_{\text{t},0}} = z_{\text{Vless}} \cdot L_{\text{Vless}} \cdot \frac{c_3^2}{2 \cdot h_{\text{t},0}}. \tag{21}$$

The flow length of each streamline through the vaneless space has been calculated as the curvature integral of a logarithmic spiral (a logarithmic spiral

has a constant angle and thus, it is the analytic solution for the flow path in a radial nozzle with isentropic and incompressible flow):

$$L_{\mathrm{Vless}} = r_3 \cdot \tan(\alpha_3) \cdot \sqrt{\left[\left(\frac{1}{\tan(\alpha_3)}\right)^2 + 1\right]} \cdot \left(\frac{r_2}{r_3} - 1\right). \tag{22}$$

The differences between flow path lengths for different VGT positions can be significant due to the growing of vaneless space outer radius and increasing flow angle when the stator vales are closing (as it can be seen in Figure 5).

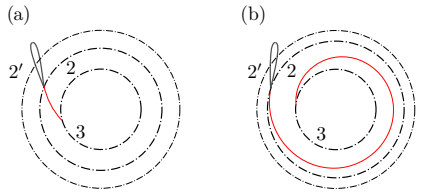

Figure 5: Vaneless space flow path with: (a) opened VGT; (b) closed VGT.

The stator outlet angle has been assumed according to Watson and Janota [7] as:

$$\alpha_3 = \arctan\left(\frac{r_2 \cdot 2\pi \cdot b_1}{z_{2'} \cdot l_{\mathrm{tho}} \cdot b_{2'}} \cdot \sin\left[\alpha_2' + \arctan\left(\frac{TE_{\mathrm{y}}}{TE_{\mathrm{x}}}\right)\right]\right). \tag{23}$$

Here, it has been necessary to adjust the stator vane angle α_2' to obtain the middle line angle at the radius of the trailing edge. The final nozzle outlet velocity has iteratively been calculated with modified Equation 17 and Equation 20, both adapted to the stations upstream and downstream the vaneless region:

$$\dot{m}_{\mathrm{red.}} = \sqrt{\frac{c_3^2}{2 \cdot h_{\mathrm{t},0}} \cdot 2 \cdot c_{\mathrm{p}}} \cdot \frac{\cos\alpha_3 \cdot A_3 \cdot C_{\mathrm{d},3}}{R} \cdot \frac{p_{\mathrm{t},2}}{p_{\mathrm{t},0}} \cdot \frac{p_{\mathrm{t},3}}{p_{\mathrm{t},2}}, \tag{24}$$

$$\frac{p_{\mathrm{t},2}}{p_{\mathrm{t},3}} = \left(\frac{1 - \frac{c_3^2}{2 \cdot h_{\mathrm{t},0}}}{1 - \frac{c_3^2}{2 \cdot h_{\mathrm{t},0}} - \frac{\Delta h_{\mathrm{Vless}}}{h_{\mathrm{t},0}}}\right)^{\frac{\gamma}{\gamma-1}}. \tag{25}$$

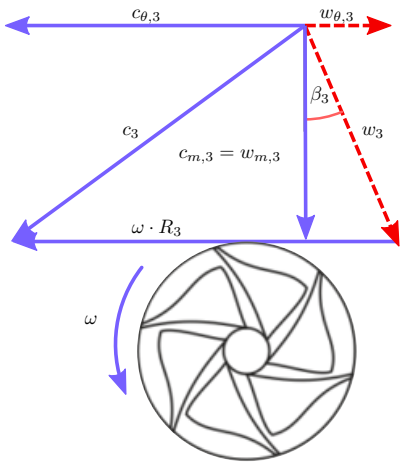

Figure 6: Rotor inlet velocity triangle.

Finally, the total stator pressure ratio can be calculated by dividing the total to static pressure ratios of stator (0-2) and vaneless space (2-3):

$$\frac{p_{\mathrm{t},0}}{p_{\mathrm{t},3}} = \frac{p_{\mathrm{t},0}}{p_{\mathrm{t},2}} \cdot \frac{p_{\mathrm{t},2}}{p_{\mathrm{t},3}}. \tag{26}$$

Following, this pressure ratio can be used to calculate the rotor pressure ratio.

2.4. Rotor

To calculate the remaining terms of the efficiency equation the rotor flow has to get resolved. Therefore, the velocity triangle in the inlet of the turbine (Figure 6) can be solved by means of already known values:

$$\frac{c_{\mathrm{m},3}^2}{2 \cdot h_{\mathrm{t},0}} = \frac{c_3^2}{2 \cdot h_{\mathrm{t},0}} \cdot \cos(\alpha_3)^2, \tag{27}$$

$$\frac{c_{\theta,3}^2}{2 \cdot h_{\mathrm{t},0}} = \frac{c_3^2}{2 \cdot h_{\mathrm{t},0}} \cdot \sin(\alpha_3)^2, \tag{28}$$

$$\frac{w_3^2}{2 \cdot h_{\mathrm{t},0}} = \left(\sqrt{\frac{c_{\theta,3}^2}{2 \cdot h_{\mathrm{t},0}}} - \sqrt{\frac{u_3^2}{2 \cdot h_{\mathrm{t},0}}} \right)^2 + \frac{c_{\mathrm{m},3}^2}{2 \cdot h_{\mathrm{t},0}}, \tag{29}$$

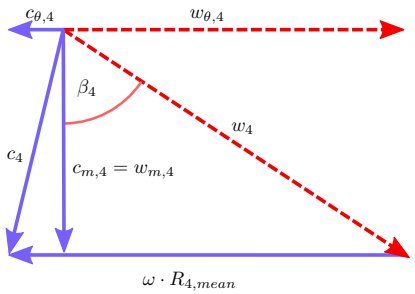

Figure 7: Rotor outlet velocity triangle.

$$\beta_3 = \arctan\left(\frac{\sqrt{\frac{c_{,3}^2}{2\cdot h_{\mathrm{t},0}}} - \sqrt{\frac{u_3^2}{2\cdot h_{\mathrm{t},0}}}}{\sqrt{\frac{c_{\mathrm{m},3}^2}{2\cdot h_{\mathrm{t},0}}}}\right). \tag{30}$$

Inlet rotational speed in non-dimensional form can be formulated as:

$$\frac{u_3^2}{2\cdot h_{\mathrm{t},0}} = \frac{\left(\frac{N_{\mathrm{red.}}}{60}\cdot \pi \cdot D_3\right)^2}{2\cdot c_{\mathrm{p}}}. \tag{31}$$

For calculating turbine outlet gas conditions in the stationary frame the rotor outlet velocity triangle, shown in Figure 7, has been solved. Since the mass flow and performance extrapolation are executed in two different models as it was done by Serrano et al. [15], the mass flow is a known variable. Thus, the equations have one degree of freedom less and the velocity triangle in Figure 7 can be calculated without assuming one blade angle and related deviation. This strategy has been chosen because current turbocharger turbines own varying trailing edge angles over the radius and thus various degrees of deviation. It is expected that the system of fitting parameters can estimate the velocity triangle in the needed accuracy. Thus, rothalpy conservation has

been used to calculate the relative outlet velocity of the rotor as:

$$\begin{aligned}\frac{w_4^2}{2 \cdot h_{\mathrm{t},0}} =& 1 - \left(\frac{p_4}{p_{\mathrm{t},3}}\right)^{\frac{\gamma-1}{\gamma}} - \frac{c_3^2}{2 \cdot h_{\mathrm{t},0}} \cdot \left[1 - \left(\frac{\cos(\alpha_3)}{\cos(\beta_3)}\right)^2\right] - \\ & - \frac{\Delta h_{\mathrm{rot.}}}{h_{\mathrm{t},0}} + \frac{u_4^2}{2 \cdot h_{\mathrm{t},0}} - \frac{u_3^2}{2 \cdot h_{\mathrm{t},0}}.\end{aligned} \tag{32}$$

The meridional velocity in the rotor outlet cross section has been calculated by means of the mass flow conservation:

$$\frac{c_{\mathrm{m},4}^2}{2 \cdot h_{\mathrm{t},0}} = \left[\frac{R \cdot \dot{m}_{\mathrm{red.}}}{A_4 \cdot d_4 \cdot \sqrt{2 \cdot c_{\mathrm{p}}}} \cdot \frac{h_4}{h_{\mathrm{t},0}} \cdot \frac{p_{\mathrm{t},0}}{p_5} \cdot \frac{p_5}{p_4}\right]^2, \tag{33}$$

while the relative static outlet enthalpy has been calculated with:

$$\frac{h_4}{h_{\mathrm{t},0}} = \left(\frac{p_4}{p_{\mathrm{t},3}}\right)^{\frac{\gamma-1}{\gamma}} + \frac{\Delta h_{\mathrm{rot.}}}{h_{\mathrm{t},0}}. \tag{34}$$

The outlet rotational speed has been calculated with:

$$\frac{u_4^2}{2 \cdot h_{\mathrm{t},0}} = \frac{\left(\frac{N_{\mathrm{red.}}}{60} \cdot \pi \cdot \bar{D}_4 \cdot DC_4\right)^2}{2 \cdot c_{\mathrm{p}}}. \tag{35}$$

Also in the rotor outlet a discharge coefficient has been used. However, it has been adjusted on the needs of a rotating system with rather radially distributed velocity field. Hence, the effective mean diameter $\bar{D}_4$ has been adjusted according to the discharged area as it can be seen in Figure 8. Due to the definition in Equation 36, the mean diameter separates always 50 % of the radially discharged area.

$$\begin{aligned}&\text{for } DC_4 > 1: \\ &C_{\mathrm{d},4} = \frac{\left(D_{4,\mathrm{out}}^2 - \bar{D}_4^2 \cdot {DC_4}^2\right) \cdot \pi}{2 \cdot A_4} \\ &\text{for } DC_4 < 1: \\ &C_{\mathrm{d},4} = \frac{\left(\bar{D}_4^2 \cdot {DC_4}^2 - D_{4,\mathrm{in}}^2\right) \cdot \pi}{2 \cdot A_4}\end{aligned} \tag{36}$$

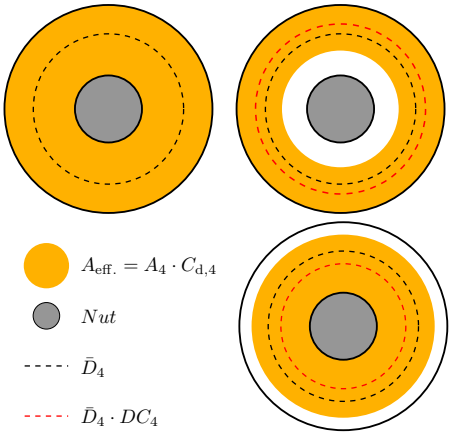

Figure 8: Rotor outlet discharge definition.

The rotor losses are sub-divided into incidence losses, passage losses, and tip leakage losses. The models for the rotor incidence and rotor passage losses by Futral et al. [24], which are well validated in the literature, are used for the rotor inside of the rotational reference frame.

$$\frac{\Delta h_{\text{rot.,inc}}}{h_{\text{t,0}}} = \sin(\beta_3 - \beta_{3,\text{opt.}})^2 \cdot \frac{w_3^2}{2 \cdot h_{\text{t,0}}} \tag{37}$$

$$\frac{\Delta h_{\text{rot.,pas.}}}{h_{\text{t,0}}} = z_{\text{rot.,pas.}} \cdot \left[\cos(\beta_3 - \beta_{3,\text{opt.}})^2 \cdot \frac{w_3^2}{2 \cdot h_{\text{t,0}}} + \frac{w_4^2}{2 \cdot h_{\text{t,0}}}\right] \tag{38}$$

Here, the optimum inflow angle $\beta_{3,\text{opt.}}$ has been estimated by the slip-factor definition of Chen and Baines [25].

For the rotor tip leakage loss model the model implemented by Serrano et al. [23] has been used. Tip leakage losses are calculated dependent on incidence and friction driven tip leakage flow momentum $(-)$, which is high in off-design conditions and dependent on pressure driven tip leakage flow momentum $(+)$:

$$\frac{\Delta h_{\text{rot.,tip}}}{h_{\text{t,0}}} = \frac{\dot{m}_{\text{cl.,}-}}{\dot{m}_{\text{turb.}}} \cdot \frac{w_{\text{cl.,`,}-}^2}{2 \cdot h_{\text{t,0}}} + \frac{\dot{m}_{\text{cl.,}+}}{\dot{m}_{\text{turb.}}} \cdot \frac{w_{\text{cl.,`,}+}^2}{2 \cdot h_{\text{t,0}}}. \tag{39}$$

Modeled velocities own one fitting coefficient for each velocity component.

$$
\begin{aligned}
w_{\mathrm{cl.,\grave{},+}} =& \frac{\left[\frac{\bar{r}_{\mathrm{sh.}}^2-\bar{r}_{\mathrm{tip}}^2}{2\cdot\bar{r}_{\mathrm{tip}}^2}+\ln\left(\frac{\bar{r}_{\mathrm{tip}}}{\bar{r}_{\mathrm{sh.}}}\right)\right]}{\left(\frac{\bar{r}_{\mathrm{sh.}}}{\bar{r}_{\mathrm{tip}}^2}-\frac{1}{\bar{r}_{\mathrm{sh.}}}\right)}\cdot \\
&\cdot\left[-\frac{1}{2}\frac{1}{\mu}\frac{\Delta p_{(\mathrm{PS,SS})}}{\Delta\theta\Delta\bar{r}_{\mathrm{tip}}}\bar{r}_{\mathrm{sh.}}\ln\left(\frac{\bar{r}_{\mathrm{sh.}}}{\bar{r}_{\mathrm{tip}}}\right)\right]+\left[\frac{\bar{r}_{\mathrm{tip}}^2-\bar{r}_{\mathrm{sh.}}^2}{4}+\frac{\bar{r}_{\mathrm{sh.}}^2}{2}\cdot\ln\left(\frac{\bar{r}_{\mathrm{sh.}}}{\bar{r}_{\mathrm{tip}}}\right)\right]\cdot \\
&\cdot\frac{1}{2}\frac{1}{\mu}\frac{\Delta p_{(\mathrm{PS,SS})}}{\Delta\theta\Delta\bar{r}_{\mathrm{tip}}}, \\
&\text{with: } \bar{r}_{\mathrm{sh.}}=\bar{r}_{\mathrm{tip}}+K_+\cdot\Delta\bar{r}_{\mathrm{tip}},
\end{aligned}
\tag{40}
$$

$$
w_{\mathrm{cl.,\grave{},-}} = K_-\cdot\frac{\left[\frac{\bar{r}_{\mathrm{sh.}}^2-\bar{r}_{\mathrm{tip}}^2}{2\cdot\bar{r}_{\mathrm{tip}}^2}+\ln\left(\frac{\bar{r}_{\mathrm{tip}}}{\bar{r}_{\mathrm{sh.}}}\right)\right]}{\left(\frac{\bar{r}_{\mathrm{sh.}}}{\bar{r}_{\mathrm{tip}}^2}-\frac{1}{\bar{r}_{\mathrm{sh.}}}\right)}\cdot\frac{\omega\cdot\bar{r}_{\mathrm{sh.}}}{\Delta\bar{r}_{\mathrm{tip}}}. \tag{41}
$$

It has been proven to have good extrapolation capability and requires only one set of coefficients for different VGT positions, speeds, and a wide range of pressure ratios. All these sub-models own fitting coefficients, which need to be fitted by means of experimental data. Finally, the outlet velocity triangle has been solved with:

$$
\frac{w_{\grave{},4}^2}{2\cdot h_{\mathrm{t},0}} = \frac{w_4^2}{2\cdot h_{\mathrm{t},0}} - \frac{c_{\mathrm{m},4}^2}{2\cdot h_{\mathrm{t},0}}, \tag{42}
$$

$$
\frac{c_{\grave{},4}^2}{2\cdot h_{\mathrm{t},0}} = \left(\sqrt{\frac{w_{\grave{},4}^2}{2\cdot h_{\mathrm{t},0}}}-\sqrt{\frac{u_4^2}{2\cdot h_{\mathrm{t},0}}}\right)^2, \tag{43}
$$

$$
\frac{c_4^2}{2\cdot h_{\mathrm{t},0}} = \frac{c_{\grave{},4}^2}{2\cdot h_{\mathrm{t},0}} + \frac{c_{\mathrm{m},4}^2}{2\cdot h_{\mathrm{t},0}}. \tag{44}
$$

2.5. Outlet

The pressure ratio between turbine rotor trailing edge up to the measurement duct has been calculated. Since the circulation in the turbine outlet is of high importance in off-design conditions towards high BSR [26], all

conservation equations have to be considered for modeling the static outlet pressure ratio. Thus, the following conservation equations are solved in non-dimensional form:

$$\frac{c_{5,\mathrm{t}}^2}{2 \cdot h_{\mathrm{t},0}} = \frac{\bar{D}_4^2}{\bar{D}_5^2} \cdot \frac{c_{4,\mathrm{t}}^2}{2 \cdot h_{\mathrm{t},0}}, \tag{45}$$

$$\frac{c_5^2}{2 \cdot h_{\mathrm{t},0}} = \frac{c_{5,\mathrm{t}}^2}{2 \cdot h_{\mathrm{t},0}} + \frac{c_{5,\mathrm{m}}^2}{2 \cdot h_{\mathrm{t},0}}, \tag{46}$$

$$\frac{h_5}{h_{\mathrm{t},0}} = \frac{h_4}{h_{\mathrm{t},0}} + \frac{c_4^2}{2 \cdot h_{\mathrm{t},0}} - \frac{c_5^2}{2 \cdot h_{\mathrm{t},0}}, \tag{47}$$

$$\frac{p_4}{p_5} = \frac{A_5 + \frac{c_{5,\mathrm{m}}^2}{2 \cdot h_{\mathrm{t},0}} \cdot \frac{A_5 \cdot 2 \cdot c_\mathrm{p}}{R} \cdot \frac{h_{\mathrm{t},0}}{h_5}}{A_5 + \frac{c_{4,\mathrm{m}}^2}{2 \cdot h_{\mathrm{t},0}} \cdot \frac{A_4 \cdot 2 \cdot c_\mathrm{p}}{R} \cdot \frac{h_{\mathrm{t},0}}{h_4}}, \tag{48}$$

$$\frac{c_{\mathrm{m},5}^2}{2 \cdot h_{\mathrm{t},0}} = \frac{c_{\mathrm{m},4}^2}{2 \cdot h_{\mathrm{t},0}} \cdot \left(\frac{A_4}{A_5}\right)^2 \cdot \left(\frac{p_4}{p_5}\right)^2 \cdot \left(\frac{h_5}{h_{\mathrm{t},0}}\right)^2 \cdot \left(\frac{h_{\mathrm{t},0}}{h_4}\right)^2. \tag{49}$$

2.6. Extrapolation Solving Scheme

The model has been programmed and run in MATLAB. Each turbine section has been resolved along the flow direction. However, a iteration between outlet section and turbine wheel is needed. Further, stator, vaneless space, rotor and outlet section have coupled equations and need to be solved in an internal iterative solution themselves.

By means of a non-linear fitting the loss parameters and discharge coefficients have been found. Here, the Levenberg-Marquardt algorithm has been chosen. However, the model is robust enough to be fitted with other non-linear methods as well. During this fitting the experimental reduced mass flow has been used as data input. When the model extrapolates towards unmeasured regions of the map, mass flow extrapolation models need to be coupled. For the presented results of this paper the mass flow extrapolation model by Serrano et al. [27] has been used to obtain necessary mass flow data. Since this mass flow model requires an efficiency as input, iterations between efficiency model and mass flow model need to be executed as it is shown in Figure 9.

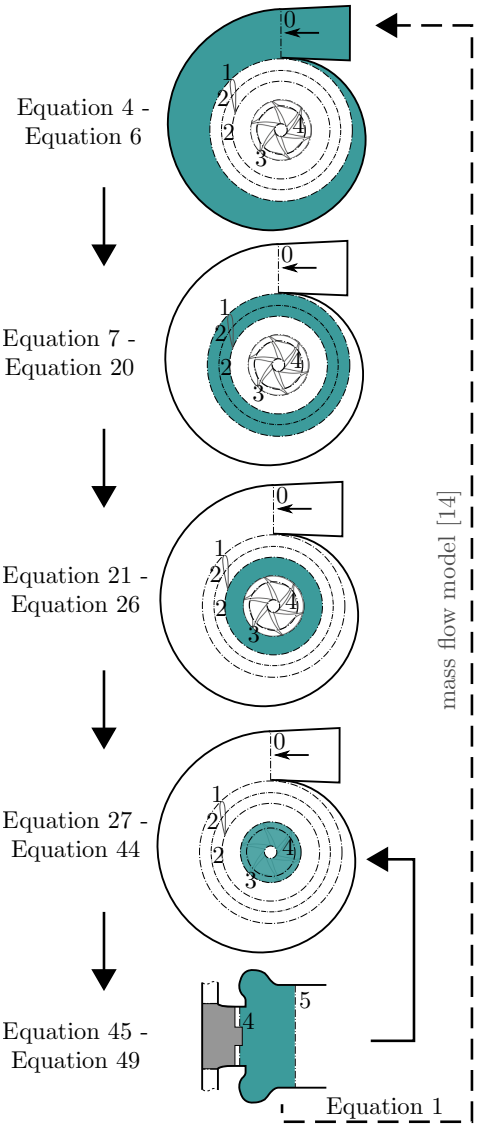

Figure 9: Solving flow chard.

3. Results & Discussion

The model has been fitted by means of the data of 3 different turbochargers (T1, T2, and T3) equipped with variable stator vanes. Each turbine has been measured at different VGT positions in quasi-adiabatic tests [10]. While T1 was measured in a wide range [10], T2 and T3 were measured in a typical narrow range of operating conditions. Further, the adiabatic efficiency has been obtained by correcting residual internal turbocharger heat fluxes by means of the heat transfer model described in [18] and [28]. For the parameter fitting only data in a typically measurable range of operating conditions has been used. Thus, all data of turbines T2 and T3 and only the 7 measurements per speedline close to the highest measured efficiency of turbine T1 are used. Each turbine has been fitted individually. The determined fitting coefficients are listed in Table 1. It can be seen that the found fitting param-

Parameter	T1	T2	T3
Stator			
$Z_{\mathrm{stat.,pass.}}$	0.27	0.31	0.74
$C_{\mathrm{d},2}$	1.00	1.00	0.60
Vaneless Space			
Z_{Vless}	0.47	0.44	0.24
$C_{\mathrm{d},3}$	0.75	0.79	0.60
Rotor			
$Z_{\mathrm{rot.,pass.}}$	0.00	0.00	0.07
$K_{\mathrm{rot.,tip,+}}$	0.04	0.04	0.05
$K_{\mathrm{rot.,tip,-}}$	1.27	1.25	1.11
DC_4	0.88	0.91	1.00

Table 1: Found fitting coefficients by non-linear fitting for three turbocharger turbines.

eters have similar magnitudes for all analyzed turbochargers. For any new turbocharger, the average of these values can be used as initial value of the parameter fitting. For T1 and T2 the new definition of the rotor outlet flow deformation has been fitted with a DC_4 value below 1. This represents a flow concentration towards the hub, which is consistent with the observation of higher $c_{4,\mathrm{m}}$ in CFD results close to design conditions. At the same time the passage loss of Equation 38 has consistently been fit with 0. Although this loss is commonly used, Meitner and Glassman [29] showed the occurrence of

high variations of this value dependent on the stator angle. Here, other loss models or the definition of the rotor outlet condition are able to compensate this loss for the desired fitting of all VGT positions. However, this might allow to reduce the model's number of fitting parameters by one.

The model is able to reproduce the turbine efficiencies in a good quality for all fitted turbines with different VGT positions and varying rotational speed, as it can be seen in Figure 10 and in Table 2. The majority of the running points are reproduced with less than 5 percentage points of error.

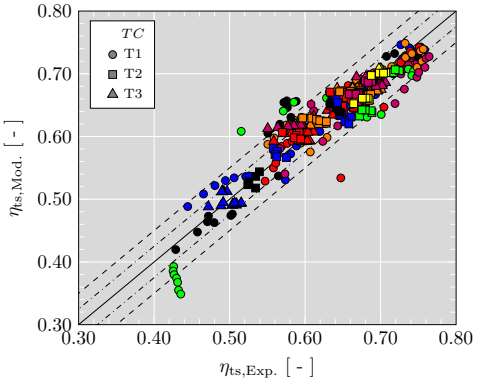

Figure 10: Overall fitting quality of T1, T2, and T3.

	T1	T2	T3
MAE	0.0258	0.0142	0.0143
RMSE	0.0332	0.0186	0.0177
Δ_{MIN}	0.11 %	0.03 %	0.03 %
Δ_{MAX}	11.34 %	5.03 %	6.22 %
R^2	0.87	0.82	0.92

Table 2: Measures of overall fitting quality of T1, T2, and T3.

After finding the fitting parameters, the aforementioned solving scheme applying a separate mass flow extrapolation model has been used to extrapolate the efficiency data. In the following, the mass flow model described in [15] has been used. In Figure 11, Figure 12, and Figure 13 the extrapolation results are shown against the BSR. It can be seen that the model is capable of reproducing the trends with VGT opening and rotational speed at the

same time for all tested turbocharger turbines. For all turbocharger turbines the following observations can be made:

1. From design condition towards off-design condition η_{ts} speedlines are further collapsing.
2. At closed VGTs: η_{ts} speedlines are wider spread; Towards opened VGTs: more and more overlapping and almost identical at very opened positions.
3. The x-axis is crossed at increasing BSR when opening the VGT.

Although all observations are qualitatively valid for the analyzed turbines, the development depends on each turbine. Comparing results for 40 % VGT opening of T2 and T3 shows different extension of the line spreading. Speedlines of T2 are spread over a much wider range of BSR than for T3 at zero efficiency. This highlights the model capability of fitting rather different turbocharger turbine behavior.

In comparison with the results of the semi-empirical model presented in [15] important differences can be highlighted. The collapsing characteristic of the data has been reproduced in more detail by the novel model. Also, the trend of stronger overlapping speedlines with the VGT opening is much better modeled in the new physical approach.

3.1. Extrapolation towards low pressure ratios

For the validation of the model extrapolation capability towards high BSR, the data has been compared against the experimental wide range data of turbine T1. To allow measurements at very low pressure ratios and very low (up to negative) turbine efficiencies, an IGV was mounted upstream the turbocharger compressor helping to convert the compressor into a centrifugal turbine [10]. The experimental measurements have very high inherent uncertainties in BSR in comparison to the turbine expansion ratio in the extrapolated zones. Hence, results are presented against the turbine expansion ratio $\pi_{\mathrm{turb.}}$ in Figure 14.

The results show good extrapolation quality towards low pressure ratios by using only a limited number of experimental points at high turbine efficiency for the model fitting (Figure 14 shows a mean absolute error (MAE) of 0.0467 and a root mean square error (RMSE) of 0.0724). The efficiency is well reproduced up to very low and even negative values. However, turbine efficiency is rather under predicted in the highest efficiency region of 6715 rpm/$\mathrm{K}^{0.5}$ measured turbo speed for the VGT openings of 30 % and 60 %.

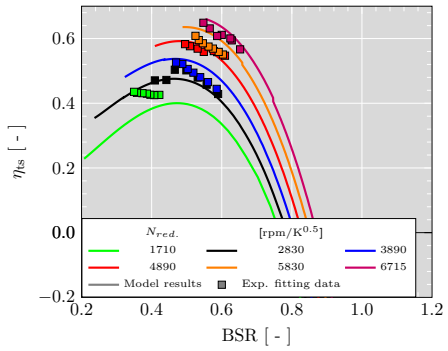

(a) Efficiency with 10 % VGT opening

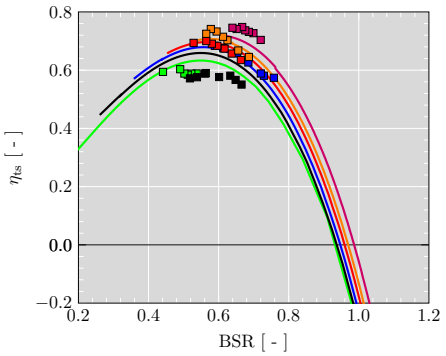

(b) Efficiency with 30 % VGT opening

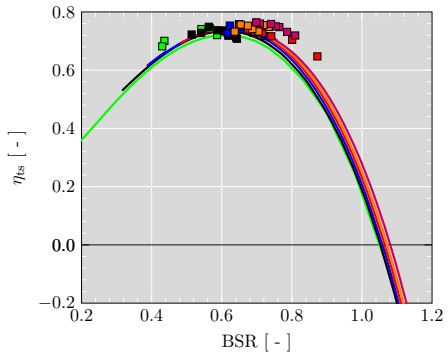

(c) Efficiency with 60 % VGT opening

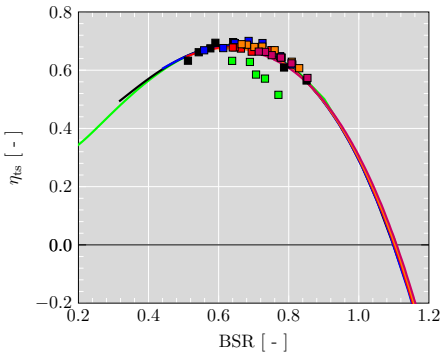

(d) Efficiency with 80 % VGT opening

Figure 11: Model fitting for turbocharger T1: η_{ts} vs. BSR.

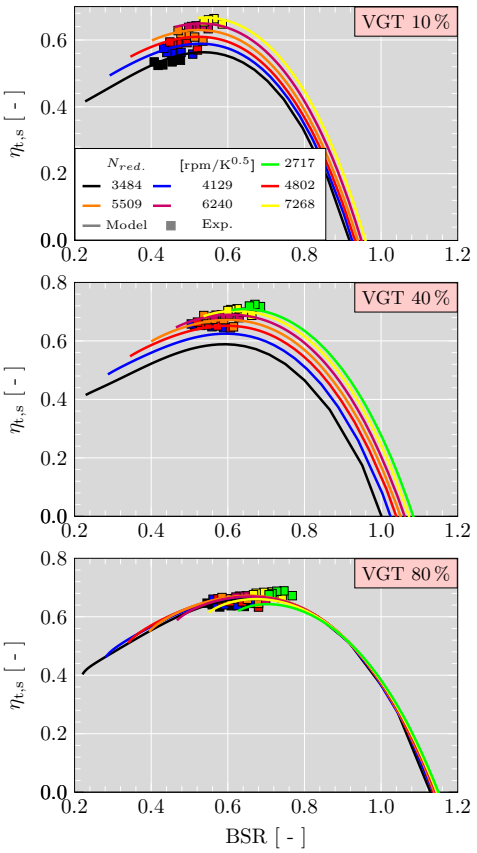

Figure 12: Model fitting for turbocharger T2: η_{ts} vs. BSR.

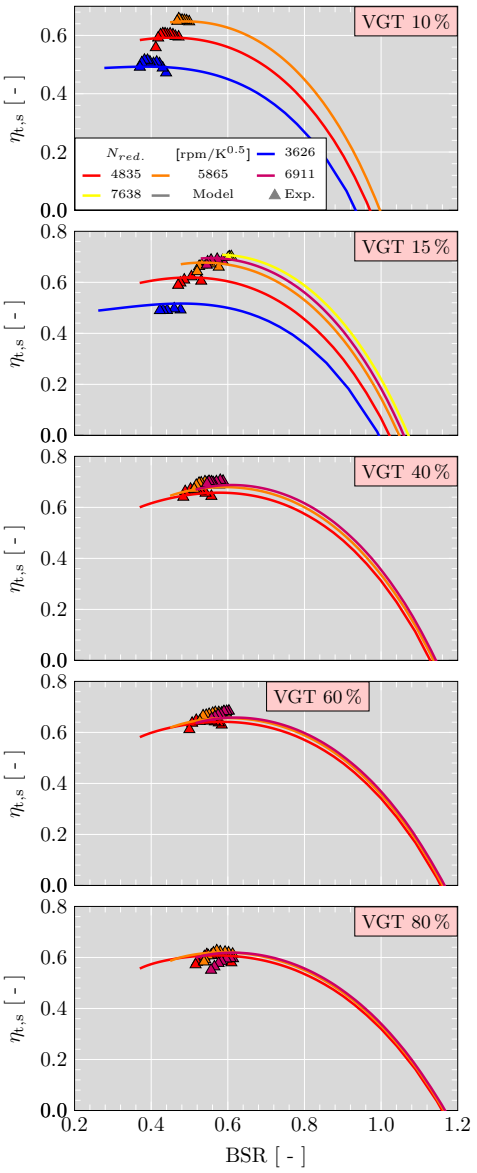

Figure 13: Model fitting for turbocharger T3: η_{ts} vs. BSR.

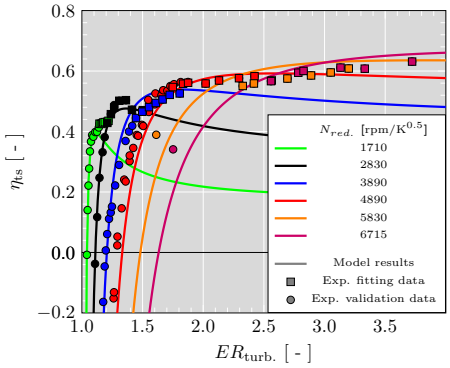

(a) Efficiency with 10 % VGT opening

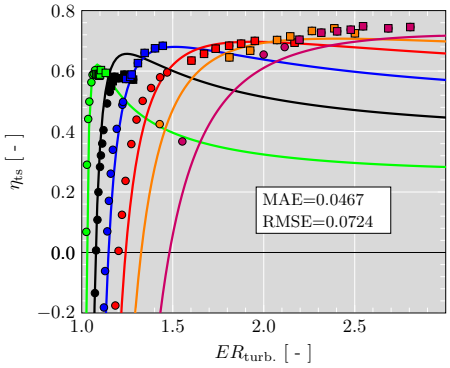

(b) Efficiency with 30 % VGT opening

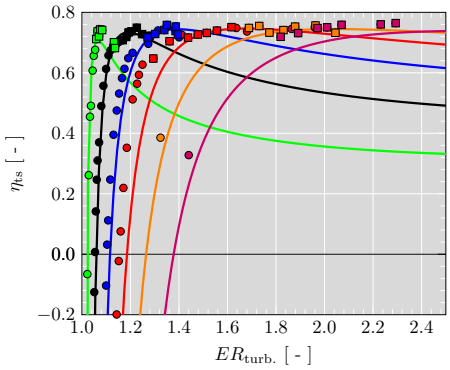

(c) Efficiency with 60 % VGT opening

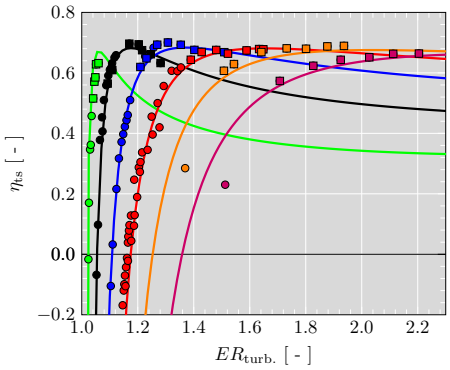

(d) Efficiency with 80 % VGT opening

Figure 14: Extrapolation towards low $ER_{\text{turb.}}$ for turbocharger T1: η_{ts} vs. $ER_{\text{turb.}}$.

Also, the second lowest speed of 30 % VGT opening seems over predicted in design condition and 4890 rpm/K$^{0.5}$ of 60 % VGT opening seems under predicted in off-design. Nevertheless, high quality of surrounding results might indicate that inherent uncertainties in the VGT mechanism are responsible for highlighted mismatch. Figure 15 shows the model results against the

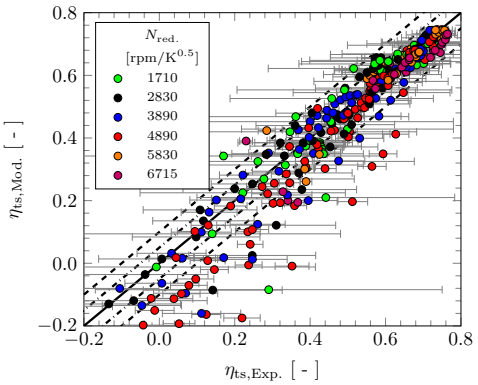

Figure 15: Model results extrapolating towards high ER vs. experimental measurements with T1.

experimental results together with the experimental errors. A more detailed analysis of experimental errors can be found in [10]. Clearly, measurement errors become very high when turbine power output is low especially in off-design conditions. This explains a certain degree of the final extrapolation error. Figure 15 also confirms that the efficiency of 4890 rpm/K$^{0.5}$ is rather under predicted. High absolute errors can occur easily due to the high slope of the curves at off-design. Hence, errors in the rotational speed can cause this kind of mismatch. All this shows the potential of this kind of models to monitor experimental measurements.

3.2. Extrapolation towards Speed

For the extrapolation towards lower and higher speeds only the experimental data of 3890 rpm/K$^{0.5}$ and 4890 rpm/K$^{0.5}$ at design condition have been used as model fitting input. These speeds are not extrapolated here. Dashed lines in Figure 16 represent the extrapolation results of Figure 14 using close to design points of all measured speeds for comparison. In Figure 16 the overall MAE of the two higher and two lower extrapolated speeds worsens from 0.0397 to 0.0479 in comparison to the fitting with all speeds (dashed lines or Figure 14). The RMSE worsens from 0.0562 to 0.0699 respectively.

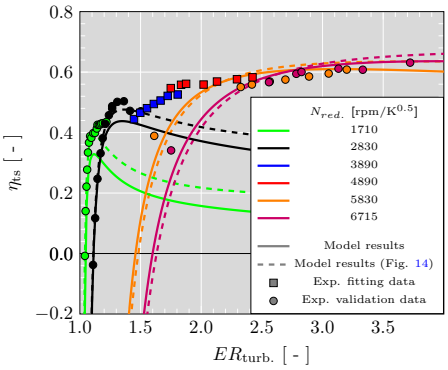

(a) Efficiency with 10 % VGT opening

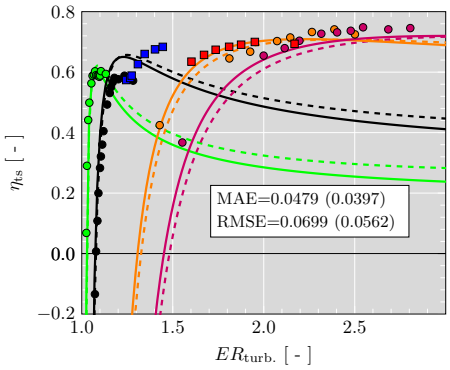

(b) Efficiency with 30 % VGT opening

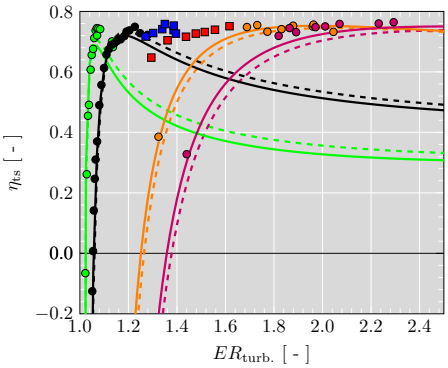

(c) Efficiency with 60 % VGT opening

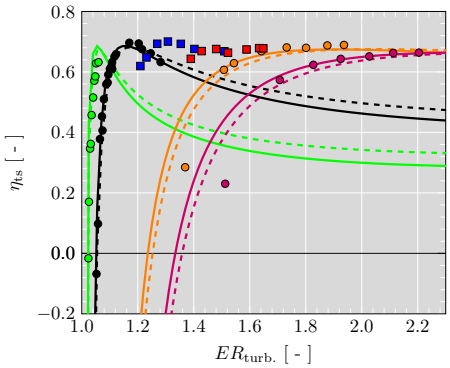

(d) Efficiency with 80 % VGT opening

Figure 16: Extrapolation towards low $ER_{\text{turb.}}$, lower, and higher speeds for turbocharger T1: η_{ts} vs. $ER_{\text{turb.}}$.

Figure 16 shows that the efficiency prediction for lower speeds has worsened slightly by under predicting the efficiency in close to design condition. However, the off-design prediction stays of the same quality. Extrapolations towards higher speeds show even a slightly better efficiency prediction for most of the points as when fitted with all speeds. Reason for this might be the fitting without the high uncertainty afflicted data of lower speedlines. In summary, fitting the model by means of only two different speeds allows to extrapolate towards higher and lower speed without loosing much quality.

3.3. Extrapolation in VGT position

The model capability of fitting several VGT positions at the same time helps to fit the loss models over a wider range. At the same time it allows to extrapolate and interpolate towards unmeasured VGT positions. Thus, this extrapolation ability has been exercised. First, the model has been fitted by means of the measurements at high efficiency of the VGT opening of 30 %, 60 %, and 80 %. With the obtained coefficients model results for the VGT position of 10 %, that are shown in Figure 17, have been generated. In respect to the fitting with all available VGT positions (dashed line) and to the experimental results, extrapolations show under predicted efficiency. While high errors can be found at low speeds, higher speeds are still well predicted. In Figure 17 the extrapolated data worsens in respect to the extrapolation with all data close to design condition (Figure 14) its MAE from 0.0401 to 0.601 and its RMSE from 0.0543 to 0.0758. Due to the high importance

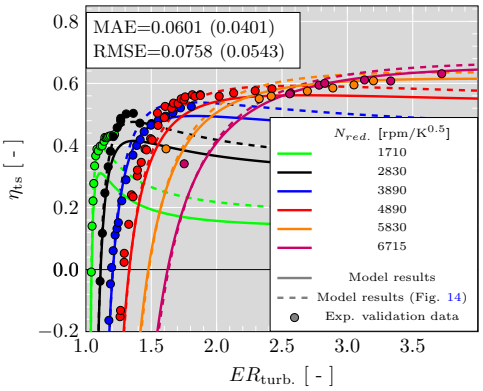

Figure 17: Extrapolation of 10 % VGT opening for turbocharger T1: η_{ts} vs. $ER_{turb.}$.

of $\frac{\Delta h_{Vless}}{h_{t,0}}$ for the fitting of all VGT maps especially at closed positions, the

fitting of this loss plays a big role when extrapolating closed VGT positions. As Figure 18 shows, described losses are progressively increasing towards closed positions. Hence, missing information in this zone complicate a good prediction of this loss. This can be understood as main limitation of the model to extrapolate with high quality.

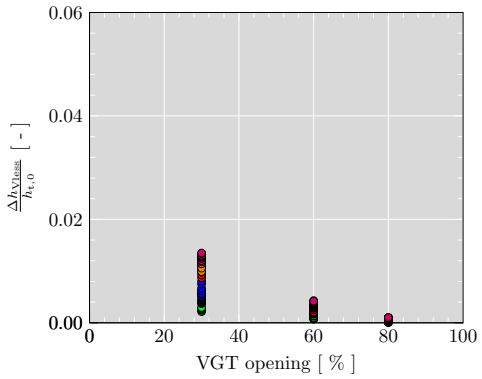

Figure 18: Modeled $\frac{\Delta h_{\mathrm{Vless}}}{h_{\mathrm{t},0}}$ fitted in design condition of 30 %, 60 %, and 80 %

Figure 19 shows the extrapolation results of 80 % VGT efficiency map. Here, the model has been fitted by the data of 10 %, 30 %, and 60 % VGT opening. It can be seen that the model results have the same quality as with the fitting of the information of all VGT positions. In Figure 19 values of MAE and RMSE barely change in comparison to the extrapolation with all data close to design condition (Figure 14).

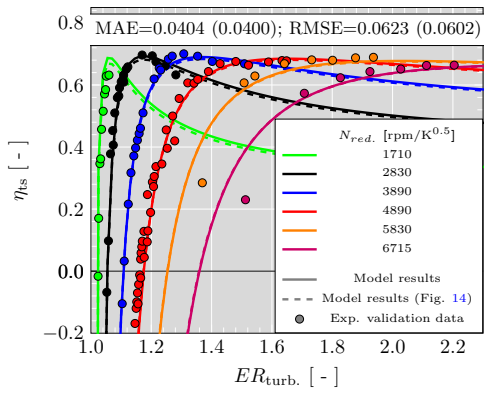

Figure 19: Extrapolation of 80 % VGT opening for turbocharger T1: η_{ts} vs. $ER_{\mathrm{turb.}}$.

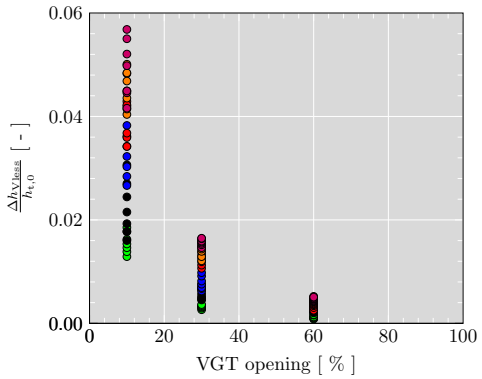

Figure 20: Modeled $\frac{\Delta h_{\mathrm{VIess}}}{h_{\mathrm{t},0}}$ fitted in design condition of 10 %, 30 %, and 60 %

In Figure 20 the fitted loss $\frac{\Delta h_{\mathrm{VIess}}}{h_{\mathrm{t},0}}$ with the three most closed VGT openings are shown. The high importance of very closed positions is clearly visible here. Since $\frac{\Delta h_{\mathrm{VIess}}}{h_{\mathrm{t},0}}$ is becoming less important for opened VGT positions, it can be expected to reliably extrapolate towards opened VGT efficiency maps.

4. Conclusion & Outlook

A one-dimensional adiabatic physically based efficiency model with novel loss correlations has been developed.

By using non-dimensional specific energies the model is independent of the turbine inlet temperature and reduced numbers can directly be used. Also, an iterative calculation of the density can be avoided in certain parts of the model.

The model owns a moderate number of fitting coefficients enhancing the stability for efficiency extrapolations.

Since the model uses the reduced mass flow as an input, equations have one degree of freedom less. Thus, for the presented model no mean blade outlet angle or outlet deviation has been estimated. The system of loss models is capable of solving the velocity triangle in the outlet of the turbine without this parameters, which might influence the result significantly.

A novel definition of the effective diameter in the rotor outlet has been given. It takes the radial distribution of the flow into account, which can be important for the energy extraction of a radial turbine.

The tip leakage model presented in [23] has been used for the first time in a complete turbine efficiency model and contributes significantly to the extrapolation quality.

The model can fit data of different VGT positions at the same time. This increases the range of mass flow and pressure ratio and thus the information that makes the data fitting and extrapolation more reliable. Here, the loss model of the vaneless space plays an important role for the VGT fitting.

Good extrapolation quality towards low pressure ratios has been stated by means of wide range experimental data. Also, the extrapolation towards higher and lower speeds can be executed in good quality. Finally, the extrapolation towards unfitted opened VGT positions can be executed in high quality.

Due to the importance of the losses in the stationary frame for the efficiency with closed VGT positions, the extrapolation towards unmeasured closed positions is challenging. Thus, it can be recommended to measure closed positions rather than extrapolating them.

The model can easily be modified to fit and extrapolate vaneless turbines, when the equations for calculating the stator outlet condition are skipped.

As the model is planned to be used in an one-dimensional entire engine simulation it needs to be solved fast. To increase the computational speed significantly the formulation of the velocities as relative kinetic energies has newly been introduced and can be used to solve the rotor by means of a system of linear equations. Further simplifications in the stator row and in the vaneless space (like assuming incompressible flow and loss calculation with isentropic velocities) can allow to solve these in a faster manner.

Acknowledgements

The work has been partially supported by the Research and Development Aid Program PAID-01-16 of the UPV.

Nomenclature

Abbreviations

BMEP	Brake Mean Effective Pressure
BSR	Blade speed ratio

DC	Diameter Correction	
ER	Expansion Ratio	
IGV	Inlet Guide Vane	
MAE	Mean Absolute Error	
RMSE	Root Mean Square Error	
TC	Turbocharger	
VGT	Variable Geometry Turbocharger	

Roman letters

A	Area	m^2
C_d	Discharge coefficient	
c	velocity in absolute reference frame	$\mathrm{m\,s^{-1}}$
c_p	Isobaric specific heat capacity	$\mathrm{J\,kg^{-1}\,K^{-1}}$
D	Diameter	m
l	length	m
h	Specific enthalpy	$\mathrm{J\,kg^{-1}}$
$\dot{m}_\mathrm{red.}$	Reduced mass flow	$\mathrm{kg\,K^{0.5}\,s^{-1}\,bar^{-1}}$
$N_\mathrm{red.}$	Reduced rotational speed	$\mathrm{rpm/K^{0.5}}$
P	Coordinates point	m
p	Pressure	Pa
$\dot{Q}$	Heat flow	W
R	Specific gas constant	$\mathrm{J\,kg^{-1}\,K^{-1}}$
R^2	Coefficient of determination	
r	Radius	m
s	Specific entropy	$\mathrm{J\,kg^{-1}\,K^{-1}}$
$sh.$	Shroud	
T	Temperature	K
$T\#$	Turbine number	
u	Uncertainty	
$\dot{W}$	Power	W
w	velocity in relative reference frame	$\mathrm{m\,s^{-1}}$
Z	Loss coefficient	

Greek letters

α	Angle in absolute reference frame	$^\circ$
β	Angle in relative reference frame	$^\circ$
γ	Heat capacity ratio	
Δ	Difference	
η	Efficiency	
ω	Angular velocity	s^{-1}

Subscripts

Roman letters

bl.	Blade
comp.	Compressor
Exp.	Experimental value
inc.	Incidence
m	Meridional component
mech.	Mechanical condition
Mod.	Model value
nut	Nut
opt.	optimum
pas.	Passage
rot.	Rotor
stat.	Stator
sh.	Shroud
t	Total or stagnation condition
ts	Total to static condition
turb.	Turbine
Vless	Vaneless space
x	x-coordinate
y	y-coordinate

Greek letters

`	Circumferential component

Numbers & Symbols

0	Turbine inlet section

1	Stator passage inlet section
2	Stator passage outlet section
3	Rotor inlet section
4	Rotor outlet section
5	Turbine outlet section
$'$	Reference to section at pivot angle in stator row
$\overline{}$	Averaged value
$\perp$	Perpendicular
$+$	Pressure driven tip leakage flow
$-$	Friction and incidence driven tip leakage flow

References

[1] Martin, G., Talon, V., Higelin, P., Charlet, A., Caillol, C.. Implementing turbomachinery physics into data map-based turbocharger models. In: J. Engines 2(1):211-229. SAE International; 2009,doi:10.4271/2009-01-0310.

[2] Rajoo, S., Romagnoli, A., Martínez-Botas, R.F.. Unsteady performance analysis of a twin-entry variable geometry turbocharger turbine. Energy 2012;38:176–189. doi:10.1016/j.energy.2011.12.017.

[3] Chiong, M.S., Rajoo, S., Martínez-Botas, R.F., Costall, A.. Engine turbocharger performance prediction: One-dimensional modeling of a twin entry turbine. Energy Conversion and Management 2012;57:68–78. doi:10.1016/j.enconman.2011.12.001.

[4] Galindo, J., Tiseira, A., Fajardo, P., García-Cuevas, L.M.. Development and validation of a radial variable geometry turbine model for transient pulsating flow applications. Energy Conversion and Management 2014;85(0):190 – 203. doi:10.1016/j.enconman.2014.05.072.

[5] Hiereth, H., Prenninger, P.. Charging the internal combustion engine. Springer Science & Business Media; 2007.

[6] Regulation (EC) No 715/2007 of the European Parliament and of the Council of 20 June 2007 on type approval of motor vehicles with respect

to emissions from light passenger and commercial vehicles (Euro 5 and Euro 6) and on access to vehicle repair and maintenance information. Official Journal of the European Union 2007;URL: http://eur-lex.europa.eu/legal-content/EN/ALL/?uri=CELEX%3A32007R0715.

[7] Watson, N., Janota, M.S.. Turbocharging the internal combustion engine. 1982. doi:https://doi.org/10.1007/978-1-349-04024-7.

[8] Serrano, J.R., García-Cuevas, L.M., Inhestern, L.B., Guilain, S., Tartoussi, H.. Analysis of unsteady energy fluxes in a turbocharger by using a holistic model extrapolating standard lookup tables in full engine operating map. In: ASME Turbo Expo 2018: Turbomachinery Technical Conference and Exposition. American Society of Mechanical Engineers; 2018, p. V008T26A015–V008T26A015. doi:doi:10.1115/GT2018-76470.

[9] Salameh, G., Chesse, P., Chalet, D.. Different measurement techniques for wider small radial performance maps. Experimental Techniques 2016;40(6):1511–1525. doi:10.1007/s40799-016-0107-8.

[10] Serrano, J.R., Tiseira, A., García-Cuevas, L.M., Inhestern, L.B., Tartoussi, H.. Radial turbine performance measurement under extreme off-design conditions. Energy 2017;125:72 – 84. doi:10.1016/j.energy.2017.02.118.

[11] Serrano, J.R., García-Cuevas, L.M., Inhestern, L.B., Mai, H., Rinaldi, A., Miguel-Sanchez, A.. Methodology to evaluate turbocharger turbine performance at high blade to jet speed ratio under quasi adiabatic conditions. In: ASME. Turbo Expo: Power for Land, Sea, and Air, Volume 8: Microturbines, Turbochargers and Small Turbomachines; Steam Turbines ():V008T26A004. American Society of Mechanical Engineers; 2017,.

[12] Baines, N.. A meanline prediction method for radial turbine efficiency. In: IMECHE conference transactions; vol. 11. Mechanical Engineering Publications; 1998, p. 45–56.

[13] Zhu, S., Deng, K., Liu, S.. Modeling and extrapolating mass flow characteristics of a radial turbocharger turbine. Energy 2015;87:628–637. doi:10.1016/j.energy.2015.05.032.

[14] Romagnoli, A., Martinez-Botas, R.. Performance prediction of a nozzled and nozzleless mixed-flow turbine in steady conditions. International Journal of Mechanical Sciences 2011;53(8):557 – 574. doi:10.1016/j.ijmecsci.2011.05.003.

[15] Serrano, J.R., Arnau, F.J., García-Cuevas, L.M., Dombrovsky, A., Tartousi, H.. Development and validation of a radial turbine efficiency model at extreme off-design conditions. Energy Conversion and Management 2016;doi:10.1016/j.enconman.2016.09.032.

[16] De Bellis, V., Bozza, F., Schernus, C., Uhlmann, T.. Advanced numerical and experimental techniques for the extension of a turbine mapping. SAE International Journal of Engines 2013;6(2013-24-0119):1771–1785.

[17] Martins, G., Mendoza, O.S.H., Tumialan, J.A.. Semi-empirical modeling of small size radial turbines for refrigeration purpose. International Compressor Engineering Conference 2006;.

[18] Serrano, J.R., Olmeda, P., Arnau, F.J., Dombrovsky, A., Smith, L.. Analysis and methodology to characterize heat transfer phenomena in automotive turbochargers. Journal of Engineering for Gas Turbines and Power 2015;137:021901–1 – 021901–11. doi:10.1115/1.4028261.

[19] Serrano, J.R., Olmeda, P., Arnau, F.J., Dombrovsky, A., Smith, L.. Turbocharger heat transfer and mechanical losses influence in predicting engines performance by using one-dimensional simulation codes. Energy 2015;86:204218. doi:10.1016/j.energy.2015.03.130.

[20] Sirakov, B., Casey, M.. Evaluation of heat transfer effects on turbocharger performance. Journal of Turbomachinery 2012;135(2). doi:10.1115/1.4006608.

[21] Serrano, J.R., Olmeda, P., Arnau, F.J., Dombrovsky, A.. General procedure for the determination of heat transfer properties in small automotive turbochargers. SAE Int J Engines 2014;8(1). doi:10.4271/2014-01-2857.

[22] Zimmermann, R., Baar, R., Biet, C.. Determine the isentropic turbine efficiency due to adiabatic measurements, and the validation of the conditions via a new criterion. In: 12th International Conference on Turbochargers and Turbocharging (17-18 May 2016, London). 2016,.

[23] Serrano, J.R., Navarro, R., Garca-Cuevas, L.M., Inhestern, L.B.. Turbocharger turbine rotor tip leakage loss and mass flow model valid up to extreme off-design conditions with high blade to jet speed ratio. Energy 2018;147(C):1299–1310. URL: https://ideas.repec.org/a/eee/energy/v147y2018icp1299-1310.html. doi:10.1016/j.energy.2018.01.

[24] Futral, S., Wasserbauer, C., Aeronautics, U.S.N., Administration, S.. Off-design performance prediction with experimental verification for a radial-inflow turbine: Samuel m.futral jr. and charles a. wasserbauer. Tech. Rep. NASA TN D-2621; NASA; 1965. URL: http://books.google.es/books?id=N1kzLAHfK-IC.

[25] Chen, H., Baines, N.. The aerodynamic loading of radial and mixed-flow turbines. International journal of mechanical sciences 1994;36(1):63–79.

[26] Serrano, J.R., Gil, A., Navarro, R., Inhestern, L.B.. Extremely low mass flow at high blade to jet speed ratio in variable geometry radial turbines and its influence on the flow pattern: A CFD analysis. In: ASME. Turbo Expo: Power for Land, Sea, and Air, Volume 8: Microturbines, Turbochargers and Small Turbomachines; Steam Turbines ():V008T26A005. American Society of Mechanical Engineers; 2017,.

[27] Serrano, J.R., Arnau, F.J., García-Cuevas, L.M., Dombrovsky, A., Tartoussi, H.. Development and validation of a radial turbine efficiency and mass flow model at design and off-design conditions. Energy Conversion and Management 2016;128:281–293.

[28] Serrano, J.R., Olmeda, P., Páez, A., Vidal, F.. An experimental procedure to determine heat transfer properties of turbochargers. Measurement Science and Technology 2010;21(3):035109. doi:10.1088/0957-0233/21/3/035109.

[29] Meitner, P., Glassman, A.. Off-design performance loss model for radial turbines with pivoting, variable-area stators 1980;.